Morphology of vacancy aggregates in carbon nanotubes: Thinning control due to interwall interaction

Mitsuru Nishikawa,[1,*] Jun-ichi Iwata,[2,3] and Atsushi Oshiyama[1,3,†]
[1]*Department of Applied Physics, The University of Tokyo, Hongo, Tokyo 113-8656, Japan*
[2]*Center for Computational Sciences, University of Tsukuba, Tsukuba 305-8577, Japan*
[3]*CREST, Japan Science and Technology Agency, Sanban-cho, Tokyo 102-0075, Japan*
(Received 11 March 2010; revised manuscript received 28 April 2010; published 27 May 2010)

We present the first-principles calculations for vacancy aggregates in carbon nanotubes which clarify relations unrecognized in the past between vacancy generation and nanomorphology. We find that the most stable form of the vacancy aggregates in single-walled carbon nanotubes (SWCNTs) is the local thinning. It is clarified that the linear vacancy in which vacant sites are topologically arranged to be parallel to the tube axis is healed in SWCNT, rendering the thinning of the vacancy area energetically favorable. In double-walled CNTs (DWCNTs), we find that the interwall interaction, which has been overlooked in the past, is decisive to determine the morphology of the vacancy aggregates. It has been clarified that wall-wall repulsive interaction suppresses the thinning due to the healing of the linear-shaped vacancy aggregates, causes limitation of the thinning, and alternatively produces the round-shaped vacancy in the outer tube. In the resultant slimmed DWCNTs, it is found that both conduction-band bottom and the valence-band top states are solely distributed on the inner tube, in contrast with normal spacing DWCNTs. This peculiar distribution in space is caused by reduction in hybridization between π orbitals and the nearly free-electron state.

DOI: 10.1103/PhysRevB.81.205442 PACS number(s): 61.46.Np, 61.72.jd, 71.15.Mb, 73.22.−f

I. INTRODUCTION

Carbon nanotubes (CNTs) (Ref. 1) exhibit fascinating electronic properties depending on their nanoscale shapes characterized by the diameter and the chirality.[2–4] Point defects such as atomic vacancies of CNT generally modulate atomic and electronic structures and then affect its properties. A lot of efforts have been indeed done[5–16] to clarify the properties related to the vacancy. Yet what is still unknown is a missing link between vacancy generation and morphology of the tube structure itself.

Electron irradiation is expected to induce vacancies in CNTs and actually exhibits rich variety of nanoshape changes, including thinning,[17–20] peeling,[21,22] and bending.[23] Mechanical stretching also induces variation in the nanoshapes and superplastic elongation of single-walled (SW) CNTs has been reported.[24,25] Interestingly, in multiwalled (MW) CNTs, no such plastic elongation has been reported. Instead, nanometer scale round-shaped vacancy aggregates at the outermost tube have been observed.[26]

In this paper, we study microscopic reason for this difference in morphology between SW- and MW-CNTs on the basis of the density-functional calculations. We first explore stable structures of multivacancies in SWCNT and clarify that the thinning or the elongation is a consequence of the stabilization of the vacancy aggregates in SWCNTs: linear-shaped vacancies are healed by reforming hexagonal networks, leading to the thinning of the vacancy area. We then reveal that the interwall repulsive interaction in double-walled (DW) CNTs suppresses the thinning and causes the round-shaped vacancy aggregates, giving rise to the morphology difference in the vacancy aggregates between SW- and MW-CNTs. This interwall interaction opens a possibility of the separation control between walls in MWCNTs via vacancy generation. It is found that electronic structure of the resultant slimmed DWCNT exhibits a new feature: carriers are confined in the inner tube.

II. CALCULATIONS

Calculations have been done with the local-density approximation (LDA) (Ref. 27) in the density-functional theory (DFT).[28] Norm-conserving pseudopotentials generated by using the Troullier-Martins scheme are adopted to describe the electron-ion interaction.[29,30] We take 0.74 Å as the core radius in generating carbon pseudopotentials. We have developed a real-space finite-difference scheme.[31–33] Our code is designed and developed for large-scale calculations on the massively parallel computers and the order N^3 operations are done with more than 80% efficiency for 10 000-atom systems using more than 1000 nodes.[33] This high performance allows us to do a large number of the accurate structural optimizations presented here. The grid spacing in the real-space calculations is taken to be 0.17 Å corresponding to a cutoff energy of 89.0 Ry, and the sixth-order finite difference is adopted for the kinetic-energy operator. We have placed a zigzag (ZZ) SW- or DW-CNT in a tetragonal cell with enough vacuum region which makes the distance between the CNT and its mirror in the neighboring cell larger than 7.0 Å. In the tube direction, a periodic unit is taken to be 4–6 times the primitive unit of the ZZ CNT in the vacancy calculations. Correspondingly we take two k points along the tube direction in the Brillouin-zone integration. Geometry optimization has been performed until the maximum force becomes less than 0.05 Ry/Å.

Interwall interaction in DWCNT includes dispersive [van der Waals (vdW)] nature for which LDA provides insufficient description. Efforts to overcome the deficiency are classified in two categories: one is the efforts to develop exchange-correlation energy functionals[34–42] and the other is

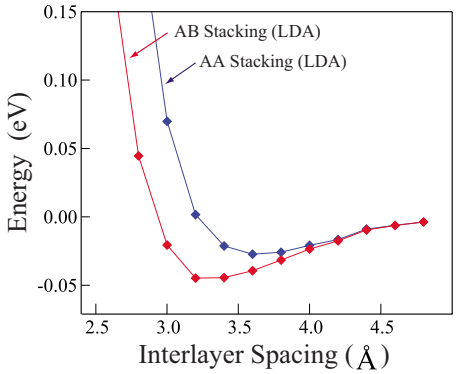

FIG. 1. (Color online) Total energy of double-layer graphene sheets per lateral unit cell as a function of layer-layer distance obtained in our LDA calculations. *AB* and *AA* stacking of the two layers are examined.

the empirical approaches[43,44] in which long-range attractive terms are added to LDA or generalized gradient approximation. Developing suitable exchange-correlation energy functional, occasionally called vdW-DFT, is of particular importance but the current approximation is not of sufficient accuracy. On the other hand, LDA provides the binding energy and the layer-layer distance for graphene sheets quite satisfactory (Fig. 1). The main deficiency in LDA, compared with the current vdW-DFT,[39] is the lack of the long-range attractive tail for the separation of layers larger than 4 Å. Since we are interested in repulsive forces induced by reduction in wall-wall distance in DWCNTs in this paper, we use LDA to discuss morphology variation in SW- and DWCNTs.

III. RESULTS AND DISCUSSION

A. Stable shapes of vacancies in SWCNT

We start with the stable structure of the vacancy V_n with n vacant sites in (10,0) SWCNT. Figure 2 shows the formation energy of $V_n(n=1-8)$.[45] For V_n with n larger than 2, there are several possibilities for the topological arrangements of the vacant sites. A particular one is the linear shape in which the vacant sites are arranged along the ZZ tube axis and the relaxation of surrounding atoms heal the linear hole perfectly

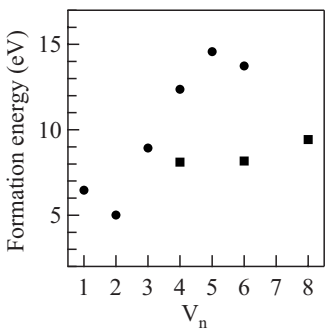

FIG. 2. Formation energy of the vacancy V_n in (10,0) SWCNT. Squares and circles denote the formation energies for linear- and round-shaped V_n.

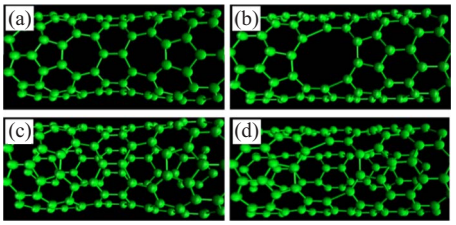

FIG. 3. (Color online) Optimized geometries of the vacancy: (a) the linear-shaped V_6 and (b) the round-shaped V_6 in (10,0) SWCNT, and (c) the linear-shaped V_6 and (d) the round-shaped V_6 in (4,0)@(10,0) DWCNT. Atoms on the backsides are not shown for clarity.

except for the two ends of the hole: at each end, five- and seven-membered rings are formed and the thinning from (10,0) to (9,0) takes place between the ends [Fig. 3(a)]. It is noteworthy that the spiral linear vacancy in chiral CNTs is also accompanied with the healing and the thinning.

Another shape is the round one in which the vacant sites gather and the surrounding atoms rebond with each other. The stable shape depends on the size of V_n and the topological arrangement of the vacant sites. We have selected plausible arrangements deduced from the calculations in the past[11,16] and optimized the geometries. Figures 3(a), 3(b), and 4 show the obtained stable round-shaped and the linear-shaped V_n with $n=1-6$. The corresponding formation energies of V_n in (10,0) SWCNT are shown in Fig. 2.

The formation energy of the linear-shaped V_n is mainly determined by the energy cost to form a pair of the five- and seven-membered rings at each end of the vacancy region. Hence the formation energy is insensitive to the size of V_n, remaining almost constant with increasing n. On the other hand, the formation energy of the round-shaped V_n tends to increase since the healing is insufficient and thus the number of weak rebonds increases with increasing n. It is thus concluded that the linear-shaped V_n is the most stable form of the vacancy aggregates in SWCNT, which explains the observed thinning of SWCNTs under electron irradiation or mechanical stretching. Superplastic elongation[24,25] may be explained in terms of diffusion of the pairs of five- and seven-membered rings as is discussed in the classical force model[12] and is corroborated by the present DFT calculations.

B. Stable shapes of vacancies in DWCNT

The energetics of the vacancy aggregates changes drastically in MWCNTs. We take (4,0)@(10,0) DWCNT as a representative of the slimmed MWCNTs in which the distance

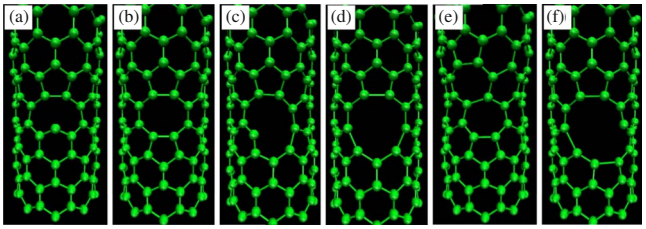

FIG. 4. (Color online) Optimized geometries of the vacancy V_n in (10,0) SWCNT. The (a) V_1, (b) V_2, (c) V_3, (d) the round-shaped V_4, (e) the linear-shaped V_4, and (f) V_5 are shown.

between the walls of the outer and the inner tubes is 2.3 Å, generate the linear- and the round-shaped V_6 on the outer tube, and have determined their stable structures. We have obtained the total-energy optimized structures, as shown in Figs. 3(c) and 3(d). The linear-shaped vacancy is perfectly healed with thinning. However its formation energy greatly increases to be 36.1 eV, being much larger than that of the round-shaped vacancy, 13.7 eV. This is a consequence of the interwall repulsive forces as will be analyzed below.

In order to analyze the interwall repulsive forces, we introduce the energy cost to make the outer tube thin in DWCNTs. In $(l,0)@(m,0)$ DWCNT, the most energetically favorable diameter of the outer tube, characterized by m_0, is determined for a fixed value of l. We have found that the interwall distance is about 3.4–3.6 Å in $(l,0)@(m_0,0)$ irrespective of the value of l. This stable distance slightly larger than the equilibrium wall-wall distance in graphite agrees with the value obtained in the previous calculation[46] and with the microscope observation.[47] Then we introduce the energy cost ΔE_t to thin the outer tube as

$$\Delta E_t \equiv E[(l,0)\ @\ (m-1,0)] - E[(l,0)\ @\ (m,0)] + n\mu_C,$$

where $E[(l,0)@(m,0)]$ is the total energy of the $(l,0)@(m,0)$ DWCNT, n is the number of removed C atoms to thin $(l,0)@(m,0)$ to $(l,0)@(m-1,0)$. In the primitive periodicity along the tube axis in $(l,0)@(m,0)$ DWCNT, n is 4. As for the chemical potential of C atom, we take the energy per atom of $(l,0)@(m,0)$ DWCNT. The competing energy cost in discussing the thinning vs the round-shaped vacancy aggregate in DWCNT is the energy cost to make the vacancy containing n vacant sites on the outer tube in $(l,0)@(m,0)$ DWCNT. We thus introduce this energy cost as

$$\Delta E_v \equiv E[(l,0)\ @\ (m,0)+V_n] - E[(l,0)\ @\ (m,0)] + n\mu_C,$$

where $E[(l,0)@(m,0)+V_n]$ is the total energy of V_n on the outer tube in $(l,0)@(m,0)$. To reduce the computational cost, we have generated a vacancy line along the tube axis without relaxation of surrounding atoms and evaluated $E[(l,0)@(m,0)+V_n]$. The resulting ΔE_v is the energy cost to generate dangling bonds on the outer tube and is regarded as an upper bound for the energy cost to generate V_n on the outer tube. The energy difference between this unrelaxed vacancy and the optimized round-shaped vacancy is estimated to be 6.0 eV.[48]

Figure 5 shows the calculated ΔE_t and ΔE_v for $(4,0)@(m,0)(m=10-14)$, $(6,0)@(m,0)(m=13-16)$, and $(8,0)@(m,0)(m=15-18)$ DWCNTs as a function of interwall distance. ΔE_t increases with the decreasing interwall distance, whereas ΔE_v remains almost constant. It is thus unequivocally shown that the thinning becomes energetically unfavorable with the interwall distance less than a certain value. We evaluate that the formation energy of a single dangling bond is about 2.5 eV and the interwall repulsion energy is less than 0.2 eV per atom. Yet all the atoms on the walls facing each other in DWCNT contribute to the repulsive energy and ΔE_t becomes larger than the energy cost to form dangling bonds locally. The competition between the weak and planar vs strong and local interactions leads to a finding that the critical distance increases with increased diameter of the inner tube, as is shown in Fig. 5.

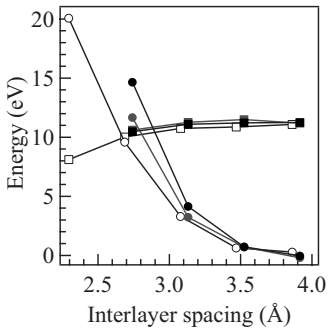

FIG. 5. Energy cost of thinning ΔE_t (circles) and of the vacancy generation ΔE_v (squares) as a function of the interwall distance in $(l,0)@(m,0)$ DWCNT. The results for $(4,0)@(m,0)(m=10-14)$, $(6,0)@(m,0)(m=13-16)$, and $(8,0)@(m,0)(m=15-18)$ DWCNTs are shown by white, gray, and black symbols, respectively.

From calculated ΔE_t and ΔE_v along with the energy difference between the unrelaxed and the round-shaped vacancy,[48] we can estimate formation energies of the linear- and the round-shaped V_6 [Figs. 3(c) and 3(d)] in (4,0)@(10,0) DWCNT. The estimated values are 36.8 eV and 13.7 eV, respectively, for the linear- and the round-shaped V_6, being close to the values obtained in our actual supercell calculations presented above.

From these calculated results, we now argue that the crossover of the formation energies between the linear- and the round-shaped V_n in DWCNT is the reason for the variation in morphology of the vacancy aggregates observed in SWCNT and in MWCNT. In SWCNTs, the generation of linear-shaped vacancy associated with self-healing leads to the thinning[17,18,23] or the elongation[24,25] of the tubes. On the other hand, in MWCNTs, the interwall repulsive interaction suppresses the thinning process beyond the critical wall-wall distance, leading to direct observation of the round-shaped vacancies.[26] Even in MWCNTs, when the linear-shaped vacancies are generated in the inner walls though it is less frequent, the thinning may take place.[19] The generation of the round-shaped vacancy is a precursor of the destruction of the outer tube. The observed peeling or sharpening in MWCNTs (Refs. 21 and 22) is presumably related to this process.

C. Electronic structures of slimmed DWCNT

The suppression of the thinning due to the interwall interaction in DWCNTs that we have found indicates that vacancy generation and successive annealing is capable of forging unusual DWCNT in which the interlayer distance is smaller by ~0.5 Å (see Fig. 5) than the most stable DWCNT. We thus explore electronic structures of such slimmed DWCNTs. Figure 6 shows calculated energy bands of the slimmed DWCNT (8,0)@(16,0) in which the interwall spacing is 3.1 Å. It is shown that each state near the energy gap is distributed exclusively in space either on the inner or

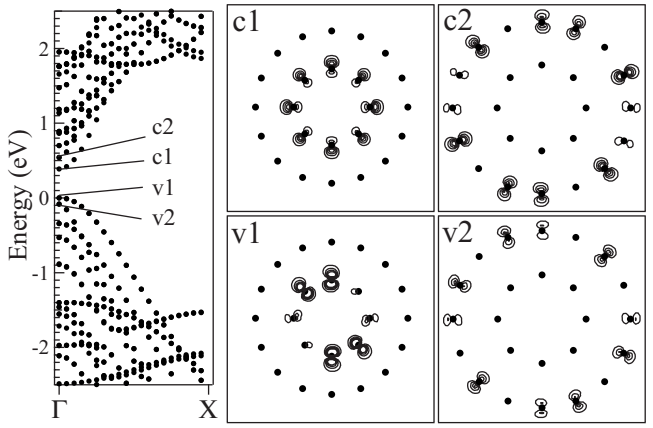

FIG. 6. Energy bands of (8,0)@(16,0) (left panel) and the projected contour plots (right panels) on the tube cross section of the Kohn-Sham orbitals of the conduction-band states (c1 and c2) and the valence-band states (v1 and v2). The c2, v1, and v2 states are all doubly degenerate. One of the doublet is plotted in each case. Dots in the right panels depict the C atomic sites. Each contour represents the density value differing from the adjacent-line value by $0.19e/\text{Å}^3$. The maximum contour represent $0.77e/\text{Å}^3$.

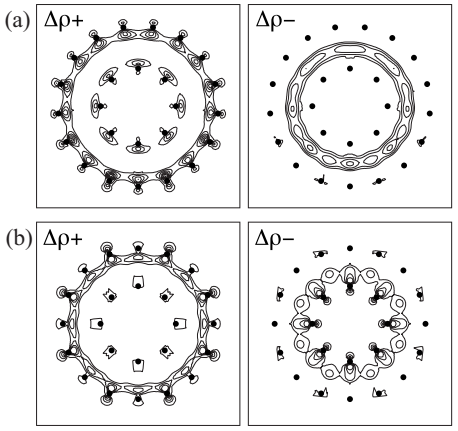

FIG. 7. Calculated charge densities on the cross-sectional plane of (a) (8,0)@(17,0) and (b) (8,0)@(16,0) DWCNTs. The positive $\Delta\rho_+$ and the negative $\Delta\rho_-$ parts of the charge density subtracted by the sum of densities of constituting SWCNTs are shown. Dots depict the C atomic sites. Each contour represents the density value differing from the adjacent-line value (a) by $0.0096e/\text{Å}^3$ or (b) by $0.019e/\text{Å}^3$. The maximum contour represent $0.077e/\text{Å}^3$.

the outer tube. But this is not new. The previous LDA calculations[46] clarified that the energy bands of the normal DWCNT with the interwall spacing of ~3.5 Å are well interpreted as a superposition of the energy bands of the inner and the outer tube with the rigid downward shift of the inner tube bands relative to the outer tube band. This is because the inner tube states contain more *s*-orbital components. As a result, the conduction-band bottom has a character of π^* of the inner tube, whereas the valence-band top is of π of the outer tube.

What is new in the slimmed DWCNT is that the both the valence-band top and the conduction-band bottom distribute on the inner tube (Fig. 6), indicative of possible control of the carrier distribution in space through slimming. Detailed analysis has clarified that the upward shift found for the inner tube state is a consequence of the induced charge polarization in the slimmed DWCNT.

The charge polarization that we have found is related to a peculiar electron state called the interlayer state or the nearly free-electron (NFE) state in carbon graphitic systems. The amplitude of the NFE state distributes not on atomic sites but in a region between atomic layers.[49–51] The NFE state is located in energy at several electron volts above the Fermi level and is detected by the photoemission spectroscopy.[52] Such states as distribute far from the atomic sites exist in spacious matters such as fullerenes[53] and carbon nanotubes.[54,55]

Figure 7 is the calculated charge densities of the slimmed and normal DWCNTs subtracted by the sum of the densities of constituting SWCNTs, $\Delta\rho=\rho_{(8,0)@(m,0)}-(\rho_{(8,0)}+\rho_{(m,0)})$. In the normal DWCNT (8,0)@(17,0) with the wall separation of ~3.5 Å, $\Delta\rho$ has negative values (electron rich) in a region between the two walls. This is due to the hybridization of the NFE states with the atomic π orbitals.[56] In the slimmed DWCNT (8,0)@(16,0), the distribution of $\Delta\rho$ is different: electrons are accumulated on π orbitals of the inner tube. This is caused by the reduced hybridization between the NFE and π states: decrease in the interwall spacing causes increase in the kinetic energy of the NFE state, hereby reduces the hybridization with the π states at the inner tube, and thus the π states are more localized near the wall of the inner tube. This localization induced by reducing the interwall spacing causes charge polarization shown in Fig. 7(b) and then modifies the energy bands: the slimming of DWCNTs transfers the electron to the inner tube with the reduction in the energy gap as is shown in Fig. 6.

IV. SUMMARY

We have performed the total-energy electronic-structure calculations for vacancy aggregates in SWCNTs and DWCNTs using our recently developed real-space scheme based on the DFT. We have found that the linear vacancy in which vacant sites are topologically arranged to be parallel to the tube axis is healed in SWCNT, leading to the thinning of the vacant region. This is because the energy cost to generate such thinning configuration is only to generate a pair of five- and seven-membered rings at each end of the thinning region. The observed thinning and elongation of SWCNT under electron irradiation is ascribed to the energetically favorable linear vacancy aggregates that we have found. In DWCNT, we have found that the interwall interaction, which has been overlooked in the past, is decisive to determine the morphology of the vacancy aggregates. It has been clarified that wall-wall repulsive interaction suppresses the thinning due to the healing of the linear-shaped vacancy aggregates and alternatively produces the round-shaped vacancy in the outer tube. This theoretical finding is consistent with the round-shaped vacancy observed recently in MWCNTs and sheds light on microscopic mechanisms for peeling of MWCNTs. The calculated energetics is indicative of possible forging of slimmed DWCNTs by electron irradiation. It is

found that both conduction-band bottom and the valence-band top states solely distribute on the inner tube in the slimmed DWCNT, in contrast with normal spacing DWCNTs, inferring a possibility of tuning the carrier distribution upon the electron irradiation. This peculiar distribution in space is caused by reduction in hybridization between π orbitals and the nearly free-electron state.

ACKNOWLEDGMENTS

Computations were performed at T2K at University of Tsukuba, and the supercomputer systems at Institute for Solid State Physics of The University of Tokyo and at Research Center for Computational Science of National Institute of Natural Science.

*Present address: Asahi Glass Co., Ltd., Japan.

†Corresponding author; oshiyama@ap.t.u-tokyo.ac.jp

[1] S. Iijima, Nature (London) **354**, 56 (1991).

[2] N. Hamada, S.-I. Sawada, and A. Oshiyama, Phys. Rev. Lett. **68**, 1579 (1992).

[3] J. W. G. Wildöer, L. C. Venema, A. G. Rinzler, R. E. Smalley, and C. Dekker, Nature (London) **391**, 59 (1998).

[4] T. W. Odom, J.-L. Huang, P. Kim, and C. M. Lieber, Nature (London) **391**, 62 (1998).

[5] A. J. Lu and B. C. Pan, Phys. Rev. Lett. **92**, 105504 (2004).

[6] A. Hashimoto, K. Suenaga, A. Gloter, K. Urita, and S. Iijima, Nature (London) **430**, 870 (2004).

[7] Y. Ma, P. O. Lehtinen, A. S. Foster, and R. M. Nieminen, New J. Phys. **6**, 68 (2004).

[8] P. O. Lehtinen, A. S. Foster, Y. Ma, A. V. Krasheninnikov, and R. M. Nieminen, Phys. Rev. Lett. **93**, 187202 (2004).

[9] S. Berber and A. Oshiyama, Physica B **376-377**, 272 (2005).

[10] A. V. Krasheninnikov, P. O. Lehtinen, A. S. Foster, and R. M. Nieminen, Chem. Phys. Lett. **418**, 132 (2006).

[11] J. Kotakoski, A. V. Krasheninnikov, and K. Nordlund, Phys. Rev. B **74**, 245420 (2006).

[12] F. Ding, K. Jiao, M. Wu, and B. I. Yakobson, Phys. Rev. Lett. **98**, 075503 (2007); F. Ding, K. Jiao, Y. Lin, and B. I. Yakobson, Nano Lett. **7**, 681 (2007).

[13] R. G. Amorim, A. Fazzio, A. Antonelli, F. D. Novaes, and A. J. R. da Silva, Nano Lett. **7**, 2459 (2007).

[14] G.-D. Lee, C.-Z. Wang, J. Yu, E. Yoon, N.-M. Hwang, and K.-M. Ho, Phys. Rev. B **76**, 165413 (2007); G.-D. Lee, C.-Z. Wang, E. Yoon, N.-M. Hwang, and K.-M. Ho, Appl. Phys. Lett. **92**, 043104 (2008).

[15] S. Berber and A. Oshiyama, Phys. Rev. B **77**, 165405 (2008).

[16] A. T. Lee, Y.-J. Kang, K. J. Chang, and I. H. Lee, Phys. Rev. B **79**, 174105 (2009).

[17] P. M. Ajayan, V. Ravikumar, and J.-C. Charlier, Phys. Rev. Lett. **81**, 1437 (1998).

[18] H. Troiani, M. Miki-Yoshida, G. A. Camacho-Bragado, M. A. L. Marques, A. Rubio, J. A. Ascencio, and M. Jose-Yacaman, Nano Lett. **3**, 751 (2003).

[19] F. Banhart, J. X. Li, and A. V. Krasheninnikov, Phys. Rev. B **71**, 241408(R) (2005).

[20] K. Asaka and T. Kizuka, Phys. Rev. B **72**, 115431 (2005).

[21] J. Cumings, P. G. Collins, and A. Zettl, Nature (London) **406**, 586 (2000).

[22] J. Y. Huang, S. Chen, S. H. Jo, Z. Wang, D. X. Han, G. Chen, M. S. Dresselhaus, and Z. F. Ren, Phys. Rev. Lett. **94**, 236802 (2005).

[23] A. Zobelli, A. Gloter, C. P. Ewels, and C. Colliex, Phys. Rev. B **77**, 045410 (2008).

[24] J. Y. Huang, S. Chen, Z. Q. Wang, K. Kempa, Y. M. Wang, S. H. Jo, G. Chen, M. S. Dresselhaus, and Z. F. Ren, Nature (London) **439**, 281 (2006).

[25] D. Bozovic, M. Bockrath, J. H. Hafner, C. M. Leiber, H. Park, and M. Tinkham, Phys. Rev. B **67**, 033407 (2003).

[26] C. Jin, K. Suenaga, and S. Iijima, Nano Lett. **8**, 1127 (2008).

[27] J. P. Perdew and A. Zunger, Phys. Rev. B **23**, 5048 (1981); D. M. Ceperley and B. J. Alder, Phys. Rev. Lett. **45**, 566 (1980).

[28] P. Hohenberg and W. Kohn, Phys. Rev. **136**, B864 (1964); W. Kohn and L. J. Sham, *ibid.* **140**, A1133 (1965).

[29] N. Troullier and J. L. Martins, Phys. Rev. B **43**, 1993 (1991).

[30] L. Kleinman and D. M. Bylander, Phys. Rev. Lett. **48**, 1425 (1982).

[31] J. R. Chelikowsky, N. Troullier, and Y. Saad, Phys. Rev. Lett. **72**, 1240 (1994).

[32] J.-I. Iwata, K. Shiraishi, and A. Oshiyama, Phys. Rev. B **77**, 115208 (2008).

[33] J.-I. Iwata, D. Takahashi, A. Oshiyama, B. Boku, K. Shiraishi, S. Okada, and K. Yabana, J. Comput. Phys. **229**, 2339 (2010).

[34] Y. Andersson, D. C. Langreth, and B. I. Lundqvist, Phys. Rev. Lett. **76**, 102 (1996).

[35] W. Kohn, Y. Meir, and D. E. Makarov, Phys. Rev. Lett. **80**, 4153 (1998).

[36] E. Hult, Y. Andersson, B. I. Lundqvist, and D. C. Langreth, Phys. Rev. Lett. **77**, 2029 (1996).

[37] M. Fuchs and X. Gonze, Phys. Rev. B **65**, 235109 (2002).

[38] M. Kamiya, T. Tsuneda, and K. Hirao, J. Chem. Phys. **117**, 6010 (2002).

[39] H. Rydberg, M. Dion, N. Jacobson, E. Schröder, P. Hyldgaard, S. I. Simak, D. C. Langreth, and B. I. Lundqvist, Phys. Rev. Lett. **91**, 126402 (2003).

[40] M. Dion, H. Rydberg, E. Schröder, D. C. Langreth, and B. I. Lundqvist, Phys. Rev. Lett. **92**, 246401 (2004); **95**, 109902(E) (2005).

[41] P. L. Silvestrelli, Phys. Rev. Lett. **100**, 053002 (2008).

[42] M. Vanin, J. J. Mortensen, A. K. Kelkkanen, J. M. Garcia-Lastra, K. S. Thygesen, and K. W. Jacobsen, Phys. Rev. B **81**, 081408(R) (2010).

[43] S. Serra, S. Iarlori, E. Tossati, S. Scandolo, and S. Santorto, Chem. Phys. Lett. **331**, 339 (2000).

[44] F. Ortmann, F. Bechstedt, and W. G. Schmidt, Phys. Rev. B **73**, 205101 (2006), and references therein.

[45] The chemical potential of carbon is taken as the energy per C atom in perfect (10,0) SWCNT. The formation energy of the linear-shaped V_8 is not converged with the supercell periodicity of 6 times the primitive unit. Additional relaxation energy is evaluated to be 0.8 eV.

[46] S. Okada and A. Oshiyama, Phys. Rev. Lett. **91**, 216801 (2003).

[47] A. Hashimoto, K. Suenaga, K. Urita, T. Shimada, T. Sugai, S. Bandow, H. Shinohara, and S. Iijima, Phys. Rev. Lett. **94**, 045504 (2005).

[48] We have examined several vacancies and found that the relaxation energy in the round-shaped V_n is about 1 eV per vacant site. We thus estimate the energy gain upon relaxation of the unrelaxed linear V_4 in the text is 6 eV since it has six dangling bonds.

[49] M. Posternak, A. Baldereschi, A. J. Freeman, E. Wimmer, and M. Weinert, Phys. Rev. Lett. **50**, 761 (1983).

[50] M. Posternak, A. Baldereschi, A. J. Freeman, and E. Wimmer, Phys. Rev. Lett. **52**, 863 (1984).

[51] N. A. W. Holzwarth, S. G. Louie, and S. Rabii, Phys. Rev. B **26**, 5382 (1982).

[52] Th. Fauster, F. J. Himpsel, J. E. Fischer, and E. W. Plummer, Phys. Rev. Lett. **51**, 430 (1983).

[53] S. Saito and A. Oshiyama, Phys. Rev. Lett. **71**, 121 (1993).

[54] Y. Miyamoto, A. Rubio, X. Blase, M. L. Cohen, and S. G. Louie, Phys. Rev. Lett. **74**, 2993 (1995).

[55] S. Okada, A. Oshiyama, and S. Saito, Phys. Rev. B **62**, 7634 (2000).

[56] S. Okada, S. Saito, and A. Oshiyama, Phys. Rev. Lett. **86**, 3835 (2001).